


Evidence to disfavour dual core system leading to double-peaked narrow emission lines

XueGuang Zhang¹ , Qi Zheng²

¹Guangxi Key Laboratory for Relativistic Astrophysics, School of Physical Science and Technology, Guangxi University, Nanning, 530004, P. R. China

²School of Physics and Technology, Nanjing Normal University, No. 1, Wenyuan Road, Nanjing, 230046, P. R. China

6 February 2023

ABSTRACT

In this manuscript, an interesting method is proposed to test dual core system for double-peaked narrow emission lines, through precious dual core system with double-peaked narrow Balmer lines in one system in main galaxy but with single-peaked narrow Balmer lines in the other system in companion galaxy. Under a dual core system, considering narrow Balmer ($H\alpha$ and $H\beta$) emissions ($f_{e, \alpha}$ and $f_{e, \beta}$) from companion galaxy but covered by SDSS fiber for the main galaxy and narrow Balmer emissions ($f_{c, \alpha}$ and $f_{c, \beta}$) from the companion galaxy covered by SDSS fiber for the companion galaxy, the same flux ratios $f_{e, \alpha}/f_{c, \alpha} = f_{e, \beta}/f_{c, \beta}$ can be expected, due to totally similar physical conditions of each narrow Balmer emission region. Then, the precious dual core system in SDSS J2219-0938 is discussed. After subtracting pPXF code determined stellar lights, double-peaked narrow Balmer emission lines are confirmed in the main galaxy with confidence level higher than 5σ , but single-peaked narrow Balmer emission lines in the companion galaxy. Through measured fluxes of emission components, $f_{e, \alpha}/f_{c, \alpha}$ is around 0.82, different from $f_{e, \beta}/f_{c, \beta} \sim 0.52$, to disfavour a dual core system for the double-peaked narrow Balmer emission lines in SDSS J2219-0938.

Key words: galaxies:nuclei - galaxies:emission lines - galaxies:individual (SDSS J2219-0938)

1 INTRODUCTION

Dual core systems on scale of dozens to thousands parsecs to supermassive binary black hole (BBH) systems on scale of sub-parsec in galaxies are commonly expected products by merging of galaxies, essential process of galaxy formation and evolution (Begelman et al. 1980; Kauffmann et al. 1993; Silk & Rees 1998; Merritt 2006; Mayer et al. 2010; Rodriguez-Gomez et al. 2017; Bottrell et al. 2019; Martin et al. 2021; Mannerkoski et al. 2022; Yoon et al. 2022). And there are many techniques proposed to detect dual core systems and BBH systems. Applications of double-peaked features of broad and/or narrow emission lines can be found in Komossa et al. (2008); Boroson & Lauer (2009); Shen & Loeb (2010); Popovic (2012); Comerford et al. (2013); Liu et al. (2016); De Rosa et al. (2019). Applications of spatially resolved image properties of central regions have been reported in Komossa et al. (2003); Rodriguez et al. (2009); Piconcelli et al. (2010); Nardini (2017); Kollatschny et al. (2020). Applications of different line profiles of broad Balmer emission lines can be found in Zhang (2021d). Applications of long-standing Optical Quasi-Periodic Oscillations have been reported in Graham et al. (2015); Kovacevic et al. (2019); Serafinelli et al. (2020); Liao et al. (2021); Zhang (2022).

Among the proposed techniques to detect dual core systems, application of double-peaked narrow emission lines is a very interesting topic. Zhou et al. (2004) have firstly reported a dual core system in SDSS J1048+0055 through double-peaked narrow emission lines combining with radio properties. And then, Gerke et al.

(2007) have reported a dual core system in EGSD2 J1420+5259 through double-peaked [O III] emission features combining with multi-band wavelength properties. Xu & Komossa (2009) have reported a dual core system in SDSS J1316+1753 through all narrow emission lines having double-peaked features. Liu et al. (2010) have reported dual core systems in four objects through double-peaked [O III] emission features combining properties of deep near-infrared images. McGurk et al. (2011) have reported a dual core system in SDSS J0952+2552 through its double-peaked [O III] lines combining with properties of resolved near-infrared images. Fu et al. (2011b) have reported a dual core system in SDSS J1502+1115 through double-peaked [O III] emission features and resolved radio images. Barrows et al. (2012) have shown a dual core system in CXOXB J1426+3533 through double-peaked narrow emission line features combining with properties of near-infrared adaptive optics imaging. Barrows et al. (2013) have shown that the dual core systems are favoured to the double-peaked high-ionization narrow emission lines through a sample of 131 quasars with $0.8 < z < 1.6$. Woo et al. (2014) have reported a dual core system through double-peaked narrow emission lines combining with Hubble Space Telescope imaging. Severgnini et al. (2021) have reported a favoured dual core system in SDSS J1431+4358 with double-peaked narrow emission lines. Besides the discussed individual objects, there are large samples of objects with double-peaked narrow emission lines reported in Smith et al. (2010); Ge et al. (2012); Wang et al. (2019), etc..

However, there are some further reports to disfavour the double-peaked narrow emission lines as efficient signs of dual core systems. Liu et al. (2010) have shown double-peaked features due to narrow-line region kinematics or dual core systems. Rosario et al. (2010)

* Contact e-mail: xgzhang@gxu.edu.cn

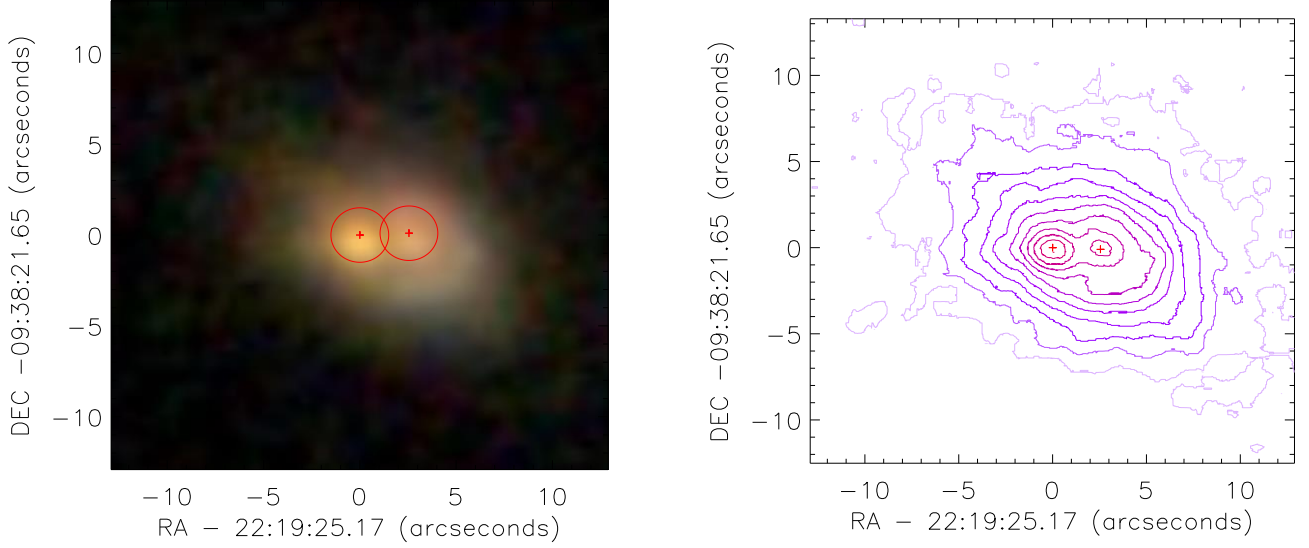


Figure 1. Left panel shows the 25.8'' \times 25.8'' colorful photometric image of SDSS J2219-0938, right panel shows corresponding brightness contour of the photometric image. In left panel, the two red circles with radii 1.5'' represent covering regions of the SDSS fibers, the two red pluses represents the pointing positions (central positions of the two nuclei) of the SDSS fibers. In right panel, the two red pluses mark the central positions of the two nuclei.

have shown double-peaked narrow emission lines due to radio-jet driven outflows. [Fu et al. \(2011\)](#) have shown scenarios involving a single AGN leading to the same double-peaked narrow emission lines. [Shen et al. \(2011\)](#) have shown kinematics scenario with a single AGN can be commonly applied for the majority of double-peaked [O III] lines in Type-2 AGN. [Fu et al. \(2012\)](#) have discussed that only probably 1% dual AGN can lead to double-peaked narrow emission lines. [Zhang \(2015\)](#) have reported non-kinematic model for double-peaked narrow H α . [McGurk et al. \(2015\)](#) have shown that only one dual core system is detected among 12 candidates with double-peaked narrow emission lines, followed by [Muller-Sanchez et al. \(2015\)](#); [Nevin et al. \(2016\)](#). [Zhang & Feng \(2016\)](#) have shown that dual core systems are not statistically preferred to double-peaked narrow emission lines, through virial BH mass comparisons of broad line AGN with and without double-peaked narrow emission lines. [Liu et al. \(2018\)](#) have shown that radio-loud double-peaked narrow emission line AGN should be related to jets.

In the manuscript, an interesting method is proposed to test the dual core system for the double-peaked narrow emission lines. Section 2 presents our main hypotheses. Section 3 presents main results and necessary discussions in the precious dual core system in SDSS J221924.98-093821.6 (=SDSS J2219-0938). Section 4 gives final conclusions. And, the cosmological parameters have been adopted as $H_0 = 70 \text{ km} \cdot \text{s}^{-1} \text{ Mpc}^{-1}$, $\Omega_\Lambda = 0.7$ and $\Omega_m = 0.3$.

2 MAIN HYPOTHESES

The main considering point is that narrow Balmer emission line regions covered by SDSS fiber have totally the same physical conditions. Then, a kind of precious dual core system, one core with double-peaked narrow Balmer emission lines in the main galaxy but the other core with single-peaked narrow Balmer emission lines in the companion galaxy, can be well discussed.

For the double-peaked narrow Balmer emission lines (H α and H β) in the main galaxy, the blue-shifted (or red-shifted) components of the

double-peaked narrow Balmer lines definitely include contributions of the narrow Balmer emissions from the companion galaxy but covered by the fiber for the main galaxy, under the framework of a dual core system. In other words, from the intrinsic narrow Balmer emission line regions of the companion galaxy, one region (ext-emission region) is covered by the SDSS fiber for the main galaxy, the other one region (comp-emission region) is covered by the SDSS fiber for the companion galaxy. Considering $p1$ and $p2$ as the ratio of narrow Balmer emissions in ext-emission region and in comp-emission region to the intrinsic total narrow Balmer emissions in the companion galaxy, we will have

$$\frac{f_{e,\alpha}}{f_{T,\alpha}} = p1, \quad \frac{f_{e,\beta}}{f_{T,\beta}} = p1, \quad \frac{f_{c,\alpha}}{f_{T,\alpha}} = p2, \quad \frac{f_{c,\beta}}{f_{T,\beta}} = p2 \quad (1)$$

with $f_{e,\alpha}$ and $f_{e,\beta}$ ($f_{c,\alpha}$ and $f_{c,\beta}$) as line fluxes of narrow H α and narrow H β from the ext-emission region (the comp-emission region), and $f_{T,\alpha}$ and $f_{T,\beta}$ as intrinsic total line fluxes of narrow H α and narrow H β of the companion galaxy. Although $p1$ and $p2$ are unknown parameters, the equations above can well lead to

$$\frac{p1}{p2} = \frac{f_{e,\alpha}}{f_{c,\alpha}} = \frac{f_{e,\beta}}{f_{c,\beta}} = R_{ec} \quad (2)$$

Therefore, properties of R_{ec} can be well applied to test the assumed dual core system for double-peaked narrow emission lines.

Certainly, due to different locations of ext-emission region and comp-emission region, different dust obscurations should have effects on the flux ratio R_{ec} . However, considering intrinsic narrow Balmer decrement (flux ratio of narrow Balmer emission lines) can be totally applied to correct the effects of dust obscurations. Then, in the manuscript, an interesting target SDSS J2219-0938 is collected and discussed, due to its double-peaked narrow Balmer emission lines in the main galaxy but single-peaked narrow Balmer emission lines in the companion galaxy.

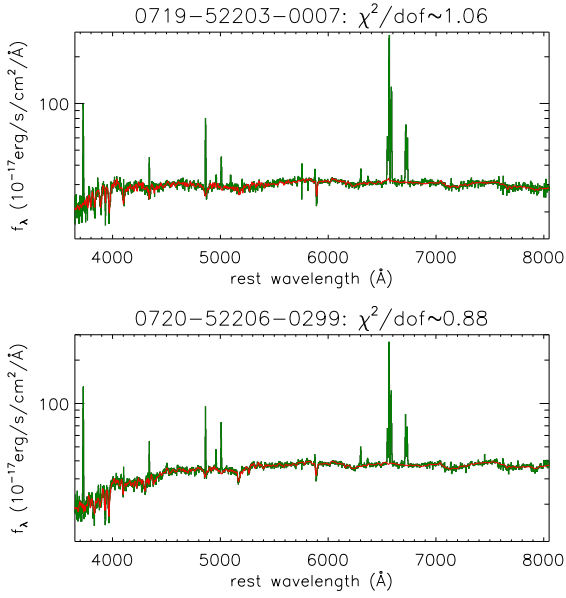


Figure 2. SDSS spectra (in dark green) of the two nuclei and the pPXF code determined host galaxy contributions (in red). The determined χ^2/dof related to the best descriptions is marked in title of each panel.

3 PHOTOMETRIC AND SPECTROSCOPIC RESULTS IN SDSS J2219-0938

SDSS J2219-0938 at redshift 0.0948 is firstly reported with double-peaked narrow emission lines in [Ge et al. \(2012\)](#). Moreover, there are not only double-peaked narrow emission lines and apparent dual core in photometric image, but also there are SDSS providing high quality spectroscopic results of the dual core, leading to the best chance to test dual core system applied to explain the double-peaked narrow emission lines in SDSS J2219-0938, through properties of R_{ec} discussed above.

Left panel of Fig. 1 shows the $25.8'' \times 25.8''$ colorful photometric image with central position of RA=22:19:24.98 and DEC=-09:38:21.6. Right panel of Fig. 1 shows the image in contour, leading to two apparent cores with central positions (brightness peak positions) of (RA=334.8548, DEC=-9.63938) and (RA=334.8541, DEC=-9.63932) marked as red pluses, leading to the projected space distance about $2.6''$ (5480pc at redshift 0.0948) between the two nuclei. Meanwhile, the two nuclei have SDSS spectra with plate-mjd-fiberid to be 0720-52206-0299 (covered by the fiber for the companion galaxy) and 0719-52203-0007 (for the main galaxy). The SDSS fiber covered areas are marked as red circles in left panel of Fig. 1, with the central positions of the two circles as the pointing positions (totally similar as the central positions of the two nuclei) of SDSS fibers.

Fig. 2 shows SDSS spectra of the two nuclei, with signal-to-noise about 22-25. In order to show clear narrow emission line features, the more recent pPXF (penalized pixel-fitting) code ([Cappellari 2017](#)), one commonly applied SSP (Simple Stellar Population) method ([Bruzual & Charlot 2003](#); [Kauffmann et al. 2003](#)), is accepted to determine stellar contributions. The pPXF code is applied with 224 SSP templates from the MILES stellar library [Falcon-Barroso et al. et al. \(2011\)](#) with 32 stellar ages from 0.06Gyrs to 17.78Gyrs and with 7 metallicities from -2.32 to 0.22. After considering the popular regularization method, the pPXF code can give reliable and smoother star-formation histories. Fig. 2 shows the determine stellar lights in

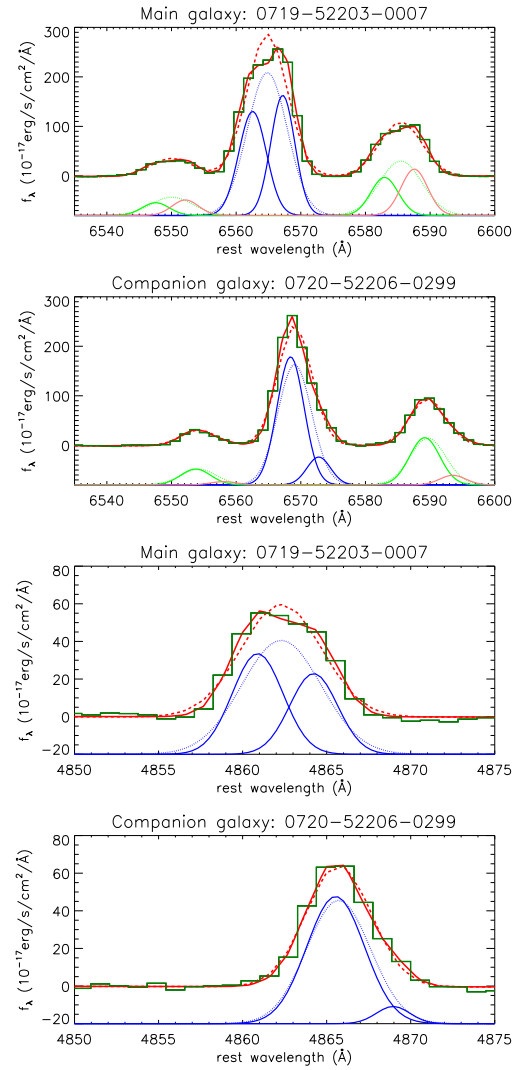


Figure 3. Top two panels show the best-fitting results (solid red line for model B, dashed red line for model A) to the emission lines around $H\alpha$ (in dark green) in the main galaxy and in the companion galaxy. Bottom two panels show corresponding results to the emission lines around $H\beta$. In top two panels, dotted blue line and dotted green lines show the model A determined narrow $H\alpha$ and $[N II]$ doublet, solid blue lines, solid green lines and solid pink lines show the model B determined Gaussian components in narrow $H\alpha$ and $[N II]$ doublet. In bottom two panels, dotted blue line shows the model A determined narrow $H\beta$, solid blue lines show the model B determined Gaussian components in narrow $H\beta$.

SDSS spectra of the two nuclei. And the pPXF code determined shifted velocities for the stellar templates are about $-17 \pm 11 \text{ km/s}$ and $-230 \pm 14 \text{ km/s}$ to describe the stellar features in the main galaxy and in the companion galaxy, respectively. The absorption features in the main galaxy are accepted to determine shifted velocities of the emission lines in the main galaxy and in the companion galaxy.

After subtracting host galaxy contributions and corrected pPXF code determined shifted properties, narrow Balmer emission lines can be well measured by multiple Gaussian functions, similar as what we have recently done in [Zhang \(2021a,b, 2022a,b,c\)](#). Emission lines around $H\alpha$ with rest wavelength from 6520 to 6620 Å are firstly discussed, including narrow $H\alpha$ and $[N II]$ doublet. In order to confirm the double-peaked narrow line emission features, two differ-

Table 1. Line parameters

line	λ_0	σ	flux	λ_0	σ	flux	λ_0	σ	flux	λ_0	σ	flux
	model A in main galaxy			model B in main galaxy			model A in companion galaxy			model B in companion galaxy		
H α	6564.8 \pm 0.1	3.1 \pm 0.1	223 \pm 2	6562.5 \pm 0.1 6567.2 \pm 0.1	2.1 \pm 0.1 1.9 \pm 0.1	112 \pm 5 113 \pm 5	6567.8 \pm 0.1	2.6 \pm 0.1	159 \pm 15	6567.1 \pm 0.1 6571.5 \pm 0.3	2.1 \pm 0.1 1.8 \pm 0.2	136 \pm 5 26 \pm 5
H β	4862.3 \pm 0.1	2.4 \pm 0.1	36 \pm 7	4860.9 \pm 0.2 4864.2 \pm 0.2	1.5 \pm 0.1 1.4 \pm 0.1	20 \pm 3 15 \pm 3	4864.7 \pm 0.1	1.9 \pm 0.1	31 \pm 7	4864.5 \pm 0.1 4867.9 \pm 0.4	1.7 \pm 0.1 1.0 \pm 0.4	29 \pm 2 2 \pm 1
[N II]	6585.4 \pm 0.1	3.3 \pm 0.1	91 \pm 10	6582.9 \pm 0.2 6587.5 \pm 0.2	2.1 \pm 0.1 2.1 \pm 0.1	41 \pm 4 48 \pm 4	6588.3 \pm 0.2	2.8 \pm 0.1	65 \pm 9	6587.8 \pm 0.2 6592.2 \pm 0.9	2.3 \pm 0.1 2.0 \pm 0.4	56 \pm 6 9 \pm 5

Notice: the center wavelength λ_0 in unit of Å, the line width (second moment) σ in unit of Å and the line flux in unit of 10^{-16} erg/s/cm².

ent model functions are applied. In model A, each narrow emission line is described by one Gaussian function. But in model B, each narrow emission line is described by two Gaussian functions. When the model functions in both model A and model B are applied, the following two criteria are accepted. First, each Gaussian component has emission flux not smaller than zero. Second, components in [N II] doublet have the same redshift, the same line width in velocity space and have the flux ratio to be fixed to the theoretical value of 3. Then, through the Levenberg-Marquardt least-squares minimization technique (MPFIT package), narrow H α and [N II] doublet can be well measured. The best fitting results are shown in top two panels of Fig. 3 with $\chi^2_A/dof_A = 1026.4/58 \sim 17.7$, $\chi^2_B/dof_B = 84.4/52 \sim 1.6$ and $\chi^2_A/dof_A = 380.8/59 \sim 6.5$, $\chi^2_B/dof_B = 87.4/53 \sim 1.6$, through applications of model A and model B to the lines in the spectra of the main galaxy and of the companion galaxy, respectively. Parameters of the emission components are listed in Table 1. In order to show clearer results in Fig. 3, the plots are limited with wavelength from 6530 to 6600 Å.

Similar as what we have recently done in Zhang (2022c), the F-test statistical technique is applied to determine whether the functions (double-peaked features) in model B are preferred in the main galaxy. Based on the different χ^2/dof values for model A and Model B, the calculated F_p value is about

$$F_p = \frac{\chi^2_A - \chi^2_B}{dof_A - dof_B} \sim 97 \quad (3)$$

Based on $dof_A - dof_B$ and dof_A as number of dofs of the F-distribution numerator and denominator, the expected value from the statistical F-test is only about 10 (very smaller than 97) with 5σ confidence level. Therefore, the confidence level is higher than 5σ to support the double-peaked narrow H α and [N II] doublet. Similar procedure is applied to the model determined results in the companion galaxy, leading to higher than 5σ confidence level to support the model B determined results. However, as listed parameters in Table 1 for emission lines in the companion galaxy, there are no reliable measurements of double-peaked features in [N II] doublet, due to measured emission intensity smaller than corresponding uncertainty. Therefore, the applied model B in the companion galaxy can lead to an extended component in narrow H α , but no double-peaked features.

Similar procedures can be applied to measure the narrow H β within rest wavelength range from 4830 to 4900 Å. Only one Gaussian component is applied in model A, and two Gaussian functions are applied in model B. Then, through the Levenberg-Marquardt least-squares minimization technique, narrow H β can be well measured. The best fitting results are shown in Fig. 3 with

$\chi^2_A/dof_A = 124.3/57 \sim 2.2$, $\chi^2_B/dof_B = 50.6/54 \sim 0.94$ and $\chi^2_A/dof_A = 60.7/58 \sim 1.0$, $\chi^2_B/dof_B = 47.3/55 \sim 0.86$, through applications of model A and model B to the lines in the spectra of the main galaxy and the companion galaxy, respectively. In order to show clearer results in Fig. 3, the plots are limited with wavelength from 4850 to 4875 Å. And the parameters of the emission components are also listed in Table 1. Furthermore, through the F-test statistical technique and the determined different χ^2/Dof values for the model A and model B, higher than 5σ confidence level can be determined to support the model B determined results in the main galaxy indicating reliable double-peaked narrow H β . Meanwhile, smaller than 3σ confidence level can be determined to support the model B determined results in the companion galaxy, moreover considering measured emission intensity smaller than 2 times of corresponding uncertainty, model A determined results are preferred in the companion galaxy, indicating single-peaked narrow H β similar as the single-peaked narrow H α in the companion galaxy.

Based on the well measured double-peaked narrow Balmer emission lines in the main galaxy but single-peaked narrow Balmer emission lines in the companion galaxy, after considering the pPXF code determined intrinsic shifted velocities in stellar features, properties of R_{ec} can be well checked. The R_{ec} in narrow H α is about $(113 \pm 5)/(136 \pm 5) \sim 0.82 \pm 0.07$, however the R_{ec} in narrow H β is about $(15 \pm 3)/(29 \pm 2) \sim 0.52 \pm 0.14$. Quite different ratios of R_{ec} in narrow H α and in narrow H β strongly indicate interesting clues not to support the assumption that the double-peaked narrow Balmer emission lines in the main galaxy are tightly related to emission regions belong to the central dual core system.

Furthermore, effects of dust obscurations can be considered as follows. The narrow Balmer emission lines have flux ratio of $5.1^{+2.1}_{-1.3}$ $((159 \pm 15)/(31 \pm 7))$ in the line spectrum of the companion galaxy. The narrow Balmer emission lines in the red-shifted components of double-peaked narrow Balmer lines in the main galaxy have flux ratio of $7.5^{+2.3}_{-1.5}$ $((113 \pm 5)/(15 \pm 3))$. The similar narrow Balmer decrements in the comp-emissions and in the ext-emissions strongly indicate similar effects of obscurations on properties of R_{ec} . Therefore, considering dust obscurations can lead to re-confirmed different R_{ec} , providing clues to disfavour the dual core system related two emission regions leading to the double-peaked narrow Balmer emission lines in the main galaxy.

4 CONCLUSIONS

Rotating dual narrow emission line regions in a dual core system can be applied to explain double-peaked narrow emission lines. However, there are more and more reports to support that double-peaked

narrow emission lines are not efficient indicators for dual core systems. Therefore, in this manuscript, an interesting and independent method is proposed to test whether the dual core system can be applied to explain double-peaked narrow emission lines in precious dual core systems with one system having double-peaked narrow emission lines but the other system having single-peaked narrow emission lines. Accepted dual core system leading to double-peaked narrow emission lines, based on measured narrow Balmer emissions ($f_{e, \alpha}$, $f_{e, \beta}$) from the emission regions of the companion galaxy but covered by the SDSS fiber for the main galaxy and measured narrow Balmer emissions ($f_{c, \alpha}$, $f_{c, \beta}$) from the emission regions of the companion galaxy covered by the SDSS fiber for the companion galaxy, it will be expected that $f_{e, \alpha}/f_{c, \alpha} = f_{e, \beta}/f_{c, \beta}$. Then, the SDSS J2219-0938 (the main galaxy) is collected, due to its double-peaked narrow Balmer emission lines and single-peaked narrow Balmer emission lines in its companion galaxy. After well measured narrow emission lines, the double-peaked narrow Balmer emission lines can be confirmed in the main galaxy with confidence level higher than 5σ . Moreover, through the measured emission components in narrow Balmer emission lines in the main galaxy and in the companion galaxy, the flux ratio $f_{e, \alpha}/f_{c, \alpha}$ is about 0.82, while the flux ratio $f_{e, \beta}/f_{c, \beta}$ is about 0.52. The results indicate that the double-peaked narrow Balmer emission lines in SDSS J2219-0938 are not mainly caused by the narrow Balmer emission line regions related to the observational dual core system. A sample of such precious dual core systems will be discussed in near future to provide further insights on dual core systems applied to explain double-peaked narrow emission lines.

ACKNOWLEDGEMENTS

Zhang & Zheng gratefully acknowledge the anonymous referee for giving us constructive comments and suggestions to greatly improve our paper. Zhang gratefully acknowledges the kind grant support from NSFC-12173020. This paper has made use of the data from the SDSS projects, <http://www.sdss3.org/>, managed by the Astrophysical Research Consortium for the Participating Institutions of the SDSS-III Collaboration, and the data from MILES library <http://miles.iac.es/>. This paper has made use of the MPFIT package <https://pages.physics.wisc.edu/~craigm/idl/cmpfit.html>, and the emcee package <https://emcee.readthedocs.io/en/stable/>. This research has made use of the NASA/IPAC Extragalactic Database (NED, <http://ned.ipac.caltech.edu>).

DATA AVAILABILITY

The data underlying this article will be shared on reasonable request to the corresponding author (aexueguang@qq.com).

REFERENCES

- Barrows, R. S.; Stern, D.; Madsen, K., et al., 2012, *ApJ*, 744, 7
- Barrows, R. S.; Sandberg Lacy, C. H.; Kennefick, J.; Comerford, J. M.; Kennefick, D.; Berrier, J. C., 2013, *ApJ*, 769, 95
- Begelman, M. C.; Blandford, R. D.; Rees, M. J., 1980, *Natur*, 287, 307
- Boroson, T. A.; Lauer, T. R. 2009, *Nature*, 458, 3
- Bottrell, C.; Hani, M. H.; Teimoorinia, H. et al., 2019, *MNRAS*, 490, 5390
- Bruzual, G.; Charlot, S. 2003, *MNRAS*, 344, 1000
- Cappellari, M., 2017, *MNRAS*, 466, 798
- Comerford, J. M.; Schluns, K.; Greene, J. E.; Cool, R. J., 2013, *ApJ*, 777, 64
- De Rosa, A.; Vignali, C.; Bogdanovic, T., et al., 2019, *NewAR*, 86, 101525
- Falcon-Barroso, J.; Sanchez-Blazquez, P.; Vazdekis, A.; et al., A&A, 2011, 532, 95
- Fu, H.; Myers, A. D.; Djorgovski, S. G.; Yan, L., 2011, *ApJ*, 733, 103
- Fu, H.; Zhang, Z.; Assef, R. J., et al., 2011b, *ApJL*, 740, 44
- Fu, H.; Yan, L.; Myers, A. D.; Stockton, A.; Djorgovski, S. G.; Aldering, G.; Rich, J. A., 2012, *ApJ*, 745, 67
- Ge, J.; Hu, C.; Wang, J.; Bai, J.; Zhang, S., 2012, *ApJS*, 201, 31
- Gerke, B. F.; Newman, J. A.; Lotz, J., et al., 2007, *ApJL*, 660, 23
- Graham, M. J.; Djorgovski, S. G.; Stern, D., et al., 2015, *Natur*, 518, 74
- Kauffmann, G.; White, S. D. M.; Guiderdoni, B., 1993, *MNRAS*, 264, 201
- Kauffmann, G.; Heckman, T. M.; Tremonti, C., et al. 2003, *MNRAS*, 346, 1055
- Kollatschny, W.; Weilbacher, P. M.; Ochmann, M. W.; Chelouche, D.; Monreal-Ibero, A.; Bacon, R.; Contini, T., 2020, A&A, 633, 79
- Komossa, S.; Burwitz, V.; Hasinger, G.; Predehl, P.; Kaastra, J. S.; Ikebe, Y., 2003, *ApJL*, 582, L15
- Komossa, S.; Zhou, H.; Lu, H. 2008, *ApJ*, 678, L81
- Kovacevic, A. B.; Popovic, L. C.; Simic, S.; Ilic, D., 2019, *ApJ*, 871, 32
- Liao, W.; Chen, Y.; Liu, X.; et al., 2021, *MNRAS*, 500, 4025
- Liu, J.; Eracleous, M.; Halpern, J. P., 2016, *ApJ*, 817, 42
- Liu, X.; Shen, Y.; Strauss, M. A.; Greene, J. E., 2010, *ApJ*, 708, 427
- Liu, X.; Greene, J. E.; Shen, Y.; Strauss, M. A., 2010, *ApJ*, 715L, 30
- Liu, X.; Lazio, T. J. W.; Shen, Y.; Strauss, M. A., 2018, *ApJ*, 854, 169
- Mannerkoski, M.; Johansson, P. H.; Rantala, A.; Naab, T.; Liao, S.; Rawlings, A., 2022, *ApJ*, 929, 167
- Martin, G.; Jackson, R. A.; Kaviraj, S., et al., 2021, *MNRAS*, 500, 4937
- Mayer, L.; Kazantzidis, S.; Escala, A.; Callegari, S., 2010, *Natur*, 466, 1082
- McGurk, R. C.; Max, C. E.; Rosario, D. J.; Shields, G. A.; Smith, K. L.; Wright, S. A., 2011, *ApJL*, 738, 2
- McGurk, R. C.; Max, C. E.; Medling, A. M.; Shields, G. A.; Comerford, J. M., 2015, *ApJ*, 811, 14
- Merritt, D., 2006, *ApJ*, 648, 976
- Muller-Sanchez, F.; Comerford, J. M.; Nevin, R.; Barrows, R. S.; Cooper, M. C.; Greene, J. E., 2015, *ApJ*, 813, 103
- Nardini, E., 2017, *MNRAS*, 471, 3483
- Nevin, R.; Comerford, J.; Muller-Sanchez, F.; Barrows, R.; Cooper, M., 2016, *ApJ*, 832, 67
- Piconcelli, E.; Vignali, C.; Bianchi, S., et al., 2010, *ApJL*, 722, L147
- Popovic, L. C., 2012, *NewAR*, 56, 74
- Rosario, D. J.; Shields, G. A.; Taylor, G. B.; Salvander, S.; Smith, K. L., 2010, *ApJ*, 716, 131
- Rodriguez, C.; Taylor, G. B.; Zavala, R. T.; Pihlstrom, Y. M.; Peck, A. B., 2009, *ApJ*, 697, 37
- Rodriguez-Gomez, V.; Sales, L. V.; Genel, S., et al., 2017, *MNRAS*, 467, 3083
- Serafinelli, R.; Severgnini, P.; Braitto, V., et al., 2020, *ApJ*, 902, 10
- Severgnini, P.; Braitto, V.; Ciccone, C., et al., 2021, A&A, 616, 153
- Shen, Y.; Loeb, A., 2010, *ApJ*, 725, 249
- Shen, Y.; Liu, X.; Greene, J. E.; Strauss, M. A., 2011, *ApJ*, 735, 48
- Silk, J. & Rees, M. J. 1998, A&A, 331, L1
- Smith, K. L.; Shields, G. A.; Bonning, E. W.; McMullen, C. C.; Rosario, D. J.; Salvander, S., 2010, *ApJ*, 716, 866
- Smith, K. L.; Mushotzky, R. F.; Boyd, P. T.; Wagoner, R. V., 2018, *ApJL*, 860, L10
- Wang, M.; Luo, A.; Song, Y., et al., 2019, *MNRAS*, 482, 1889
- Woo, J.; Cho, H.; Husemann, B.; Komossa, S.; Park, D.; Bennert, V. N., 2004, *MNRAS*, 437, 32
- Xu, D.; Komossa, S., 2009, *ApJL*, 705, 20
- Yoon, Y.; Park, C.; Chung, H.; Lane, R. R., 2022, *ApJ*, 925, 168
- Zhang, X. G., 2015, *MNRAS Letter*, 449, 31
- Zhang, X. G.; Feng L. L., 2016, *MNRAS*, 457, 3878
- Zhang, X. G., 2021m, *MNRAS*, 502, 2508
- Zhang, X. G., 2021a, *ApJ*, 909, 16, *ArXiv:2101.02465*
- Zhang, X. G., 2021b, *ApJ*, 919, 13, *ArXiv:2107.09214*
- Zhang, X. G., 2021d, *MNRAS*, 507, 5205
- Zhang, X. G., 2022a, *ApJS*, 260, 31

Zhang, X. G., 2022b, ApJS, 261, 23

Zhang, X. G., 2022c, ApJ, 937, 105, ArXiv:2209.02164

Zhang, X. G., 2022, MNRAS, 512, 1003, arXiv:2202.11995

Zhou, H., Wang, T., Zhang, X., Dong, X., Li, C. 2004, ApJL, 604, L33